BAR-ILAN UNIVERSITY

Transport and Magnetism in Conducting Perovskites

MORDEHAI (MOTY) SCHULTZ

Department of Physics

Ph.D. Thesis

Submitted to the Senate of Bar-Ilan University

Ramat-Gan, Israel January 2009

This work was carried out under the supervision of

Professor Lior Klein

Department of Physics

Bar-Ilan University

Acknowledgments

First, I would like to thank my advisor, Prof. Lior Klein, for creating rich educational environment and providing me guidance as I worked on my thesis. I am grateful to Lior for helping me to define scientific goals, and for letting me to choose my own way to achieve them.

I wish to thank the students in the group when I joined years ago who made me fill welcome. Yevgeny Kats cheerfully helped me and introduced me into experimental solid state physics. His passion to knowledge and science has been an example to me. I learned from Shahar Levi a lot about importance of accuracy, dedication and hard work in experimental physics. I would like to personally thank Michael Feigenson (the matchmaker) for teaching me everything I know about relations and electric switches.

I thank Isaschar Genish who spent long hours working with me on e-beam lithography and photolithography. I thank Yosi Basson for many useful discussions about physics, computers and life. It also has been a great pleasure to share the laboratory with Ishai Shperber, Snir Seri and Nati Naftalis.

Finally, I would like to thank my family, in particular my father of blessed memory and my mother who showed me the pleasure of finding things out and helped me and supported me all the way. I could not be where I am today were it not for their love. Last, but definitely not least, I thank my beautiful wife Keren for her support and patience over the years.

To my parents

AJZIK SCHULTZ of blessed memory and ESTER SCHULTZ

Contents

Abstract

Transition metal oxides with perovskite structure ("perovskites") attract considerable interest for the wide range of intriguing physical properties they exhibit including: high-temperature superconductivity (cuprates), colossal magnetoresistance (manganites), ferroelectricity (titanates), exotic superconductivity, itinerant magnetism and non-Fermi liquid behavior (ruthenates), etc. In addition, many of these perovskites are lattice matched due to their similar structure; hence, it is possible to grow heteroepitaxial structures consisting of various perovskites, enabling the exploration of new physical phenomena as well as the design of novel electronic devices. These features make perovskites an attractive material system for realizing all-oxide electronics. The fact that some of the perovskites are a source for highly spin-polarized current make them an interesting material system for spintronics as well.

This work focuses on studying the magnetic and transport properties of the pseudo-cubic ruthenates $CaRuO_3$ and $SrRuO_3$ thin films, and electron-doped $SrTiO_3$.

The ruthenium-based perovskites (ruthenates) provide exciting opportunities to study some of the central issues in solid state physics. The strong electron-electron correlations found in many of the metallic ruthenates give rise to anomalous transport properties that clearly deviate from conventional Fermi-liquid behavior.

In addition, the ruthenates exhibit a rich variety of electronic phases that include

itinerant magnetism (ferromagnetism, antiferromagnetism, metamagnetism) and p-wave superconductivity. The magnetism in ruthenates also has unique properties. Being a $4d$ element, ruthenium has a large spin orbit coupling constant (900 cm^{-1}, compared, e.g., to 400 cm^{-1} in iron). Consequently, properties such as magnetic anisotropy energy obtain relatively high values (usually the anisotropy field for $3d$ ferromagnets is more than an order of magnitude smaller).

The itinerant ferromagnet $SrRuO_3$ has attracted considerable interest due to its anomalous properties. Its electrical resistivity is relatively large ($\rho \sim 200$ $\mu\Omega$ cm at room temperature), and continues to grow as a function of temperature almost without saturation, and seems to cross the Ioffe-Regel limit. In addition, in the vicinity of T_c, the behavior of the temperature derivative of the resistivity strongly deviates from Fisher-Langer theory. Furthermore, terahertz conductivity and infrared conductivity are also quite anomalous, strongly indicating non-Fermi liquid behavior.

Studying the effect of film thickness on transport and magnetic properties of ruthenates films provides a new way of exploring the properties of this intriguing family of compounds. The thickness affects the electron-electron correlation, the magnetic ordering, and the effect of disorder. Studying these effects in systems that are strongly electron correlated already in their bulk form, may yield new insight into the effect of electron-electron correlations on different transport phenomena. In addition, the ultrathin films will provide new opportunities for exploring dimensional effects on magnetism in a unique example of $4d$ ferromagnetism.

In our study we explored the effects of decreasing film thickness on the transport and magnetic properties of epitaxial ultrathin films of $SrRuO_3$. We found higher re-

sistivity when the film thickness was decreased, and our analysis suggests increased effects of electron-electron correlations. We also found that the ferromagnetic phase transition occurs at a lower Curie temperature (T_c) for thinner films, and we attributed this behavior to finite size effects. The extracted critical exponents are consistent with the universality class of 3D Ising, while hints of dimensional crossover very close to T_c are not conclusive. The magnetic anisotropy is also affected by film thickness and the easy axis, normally at 45^o to the film normal, rotates towards a more perpendicular orientation, etc. This study was recently submitted to Phys. Rev. B.

To obtain more insight on the extraordinary Hall effect (EHE) mechanism in $SrRuO_3$, we examined the EHE in a different way. We studied the EHE in the ultrathin limit, thus we increased the resistivity quite significantly without inducing structural disorder. We found a low temperature range where the EHE in all the films seem to be described by a single function of ρ. On the one hand, our observation appears to be a strong confirmation of the extrinsic model which implies that R_s is a function of ρ alone. On the other hand, we saw that above a certain temperature the scaling breaks down, which may indicate that the EHE in $SrRuO_3$ is sensitive not only to the scattering rate but also to the nature of the scattering events. This study was recently accepted for publication in J. Appl. Phys.

$CaRuO_3$ is one of the most intriguing members of ruthenate perovskites. Its resistivity has a $T^{3/2}$ dependence at low temperature, suggesting a non-Fermi liquid behavior due to antiferromagnetic quantum phase transition. Optical conductivity measurements show Non-Drude behavior and specific heat measurements indicate

that electron-electron correlations in $CaRuO_3$ are even stronger than in $SrRuO_3$.

We performed extensive magnetoresistance and Hall effect measurements of untwinned epitaxial films of $CaRuO_3$. We found that at low temperatures the magnetoresistance is mainly a function of the magnitude of the magnetization. We clearly demonstrated that the susceptibility in $CaRuO_3$ is anisotropic and can be described in terms of an anisotropic susceptibility tensor. Following the identification of the magnetic properties, we found that suppression of the low temperature non-Fermi liquid behavior by external magnetic field is most efficient when the field is applied along the easy axis of magnetization; suggesting that critical spin fluctuations, possibly due to proximity of a quantum critical phase transition, are related to the non-Fermi liquid behavior. The results of this research were published in Phys. Rev. B **73**, 085109 (2006) and Physica B **378-380**, 490 (2006).

$SrTiO_3$ is another perovskite of particular interest. In addition to being considered by many an ideal insulating substrate on which epitaxial films of perovskites are grown, it now seems that electron-doped $SrTiO_3$ may also play an important role. Recent excitement in the field is related to reports on the formation of quasi two dimensional electron gas at $SrTiO_3 - LaAlO_3$ interface with very high mobilities. On the other hand, other reports claim that this is not an interface effect but a conduction of electron-doped $SrTiO_3$ formed due to oxygen vacancies in $SrTiO_3$. Irrespective of the dispute regarding the source of high mobility in $SrTiO_3 - LaAlO_3$ systems, it is clear that the electron gas in oxygen deficient $SrTiO_3$ exhibits similar mobilities which might make it an important component for spintronics with perovskites.

Electron doping $SrTiO_3$ by creating oxygen vacancies can be achieved in vari-

ous ways including high-temperature annealing in oxygen reduced pressure and Ar^+-irradiation. In our work, we electron-doped single crystal samples of $SrTiO_3$ by exposing them to Ar^+ irradiation. We found that some transport properties are time-dependent. In particular, the sheet resistance increases with time at a temperature-dependent rate, suggesting an activation barrier on the order of 1 eV. We attributed the relaxation effects to diffusion of oxygen vacancies - a process with energy barrier similar to the observed activation energy. In contrast to the resistance, the change of the mobility and the magnetoresistance (MR) with irradiation dose and relaxation time is hardly detectable. In addition, the MR data at temperatures higher than 50K obey Kohler's rule; namely, it is a function of $H \times \tau$ alone. These results suggest that the diffusion of oxygen vacancies decreases the number of charge carriers while hardly affecting the scattering rate of the remaining charge carriers. This study was published in Appl. Phys. Lett. **91**, 151104 (2007).

Chapter 1

Background

1.1 Perovskites

1.1.1 General

Perovskites, named after the Russian mineralogist, L. A. Perovski (1792-1856), are compounds with the general formula $A_{n+1}B_nO_{3n+1}$, where A and B are cations and O is an oxygen anion.[1] Transition metal perovskites exhibit intriguing properties both for application and for theoretical study: high-temperature superconductivity (cuprates) [1], colossal magnetoresistance (manganites) [2], ferroelectricity (titanates), exotic superconductivity, itinerant magnetism and non-Fermi liquid (NFL) behavior (ruthenates) [3, 4, 5], etc. In addition, epitaxially grown heterostructures of perovskites expand the range of potential functionalities beyond the range of their

[1] There are a few perovskites without oxygen, e.g., $NaMgF_3$.

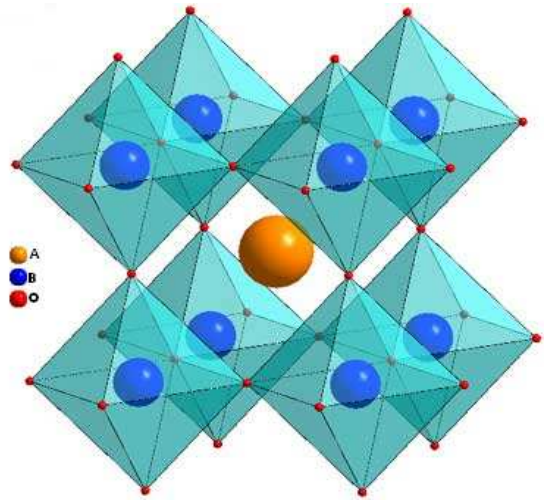

Figure 1.1: The easiest way to visualize the cubic perovskite crystalline structure.

constituents. For these reasons, it is argued that in addition to current industrial use of oxides, oxide-based electronics is one of the potential alternatives to silicon-based electronics. The fact that some of the perovskites are a source for highly spin-polarized current make them also an interesting material system for spintronics.

1.1.2 Crystalline structure

Cubic perovskites - The cubic perovskites are perovskites with $n \rightarrow \infty$ (ABO_3). The easiest way to visualize the cubic perovskite crystalline structure is in terms of the BO_6 octahedra which share corners infinitely in all 3 dimensions, making for a very nice and symmetric structure (see Figures 1.1 and 1.2(a)).

Layered Perovskites - The Layered Perovskites are perovskites with a finite n. As shown in Figures 1.2(b) and 1.2(c) the Layered perovskites consist of layers of ABO_3 type structure which are separated by some motif ("n" indicates the thickness of the ABO_3 layers).

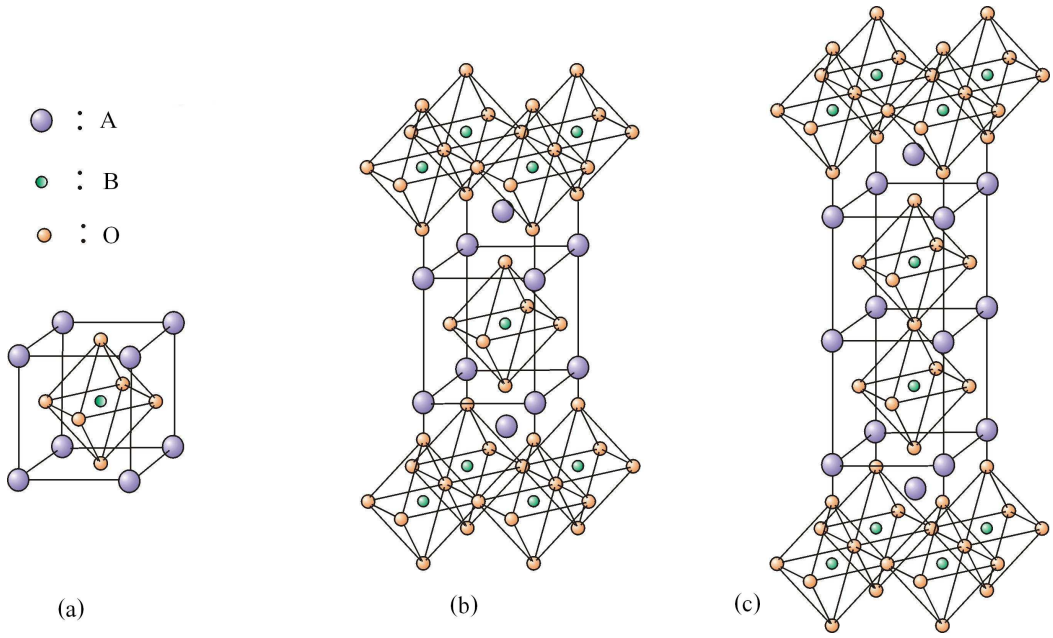

Figure 1.2: Schematic diagram of the crystalline structure of perovskites (a) Cubic perovskite ABO_3 ($n \rightarrow \infty$). (b) Layered perovskites A_2BO_4 (n=1). (c) Layered perovskites $A_3B_2O_7$ (n=2).

This work focuses on studying the magnetic and transport properties of $CaRuO_3$, $SrRuO_3$ and electron-doped $SrTiO_3$ which belong to the cubic perovskites group.

Most perovskite crystalline structures are distorted. Common distortions such as tilting of the octahedra and cation displacements within the octahedra are related to the properties of the A and B cations. Factors that contribute to distortion in the structure include radius size effects and the Jahn-teller effect. *Radius size effects* - The degree of distortion in (ABO_3) perovskites can be determined using the Goldschmodt equation:

$$t = \frac{R_A + R_O}{\sqrt{2}(R_B + R_O)} \tag{1.1}$$

where R_i is the radius of atom i. The ideal cubic perovskite has $t \approx 1$. If the A ion is smaller than the ideal value, then t becomes smaller than 1. As a result the BO_6 octahedra will tilt in order to fill space. On the other hand, if t is larger than 1 due to a large A or small B, then hexagonal variants of the perovskite structure are stable. *Jahn-teller effect* - Nonlinear molecule cannot be stable in a degenerate electronic state and must undergo distortion in order to break down the degeneracy and become stable. Distortion caused by the Jahn-Teller effect in perovskites usually involves four of the octahedral bonds contracting and two of the octahedral bond lengthening which gives an elongated octahedral shape.

At room temperature $CaRuO_3$ and $SrRuO_3$ have orthorhombically distorted perovskite structure. $CaRuO_3$ is more distorted, as expected, because Ca radius is even less ideal for perovskite formation. In contrast to $CaRuO_3$ and $SrRuO_3$, at room temperature $SrTiO_3$ exists in the cubic form, but transforms into a tetragonal structure at temperatures less than 105 K.

1.1.3 Spintronics and all oxide electronics with perovskites

One of the areas in which perovskites may play an important role is spin transport electronics ("spintronics") [6, 7, 8, 9]. Spintronics addresses phenomena sensitive to the spin of the charge carrier which arise when the electrical current is spin-polarized, as it is the case, for instance, in itinerant ferromagnets. Spintronics phenomena include giant magnetoresistance (GMR) [10], tunneling magnetoresistance (TMR) [11], spin injection [8], etc. While GMR and TMR devices have been successfully realized using magnetic and nonmagnetic metals (e.g., cobalt and copper), their integration with silicon electronics, which would have dramatically increased their impact, faces some fundamental obstacles due to conductivity mismatch [12]. Magnetic semiconductors would enable better integration with silicon electronics; therefore, the development of spintronics with these materials is a route which is vigorously explored. However, it is not clear how successful it would be due to the degree of spin polarization and the relatively low Curie temperature. Perovskites offer an alternative material system to be used for spintronics: they offer an attractive combination of high spin polarization, low carrier density and high quality interfaces. These features may enable spin injection with minimal loss of spin polarization and possibilities of spin manipulation with gate voltage application. Recently, there have been several reports on spintronics devices consisting of perovskites [13, 14, 15]. These reports highlight the potential contribution of perovskites to the emerging field of spintronics.

The development of devices based on ultrathin films is an active area of research. $SrRuO_3$ is an itinerant ferromagnet with Curie temperature of 150 K. While this

compound is not likely to be relevant for spintronics applications due to its relatively low Curie temperature, it is a compound that allows the study of basic spintronics effects due to its special features. In particular, it has very high uniaxial magnetocrystalline anisotropy (anisotropy field of about 10 T) which is responsible for a stripe domain structure with extremely narrow domain walls ($\sim$ 3 nm in width). These features make this compound an ideal model system for studying spin transport in the presence of magnetic interfaces such as: current-induced domain wall motion [16] and interface resistance of domain walls [17]. In addition, $SrRuO_3$ can be used in future all oxide electronics device applications due to its chemical stability, metalic conductivity, and epitaxial growth on perovskite substrates. Therefore, it is important to understand the magnetotransport properties of ultrathin films of $SrRuO_3$.

Electron-doped $SrTiO_3$ yields high mobilities on the order of $10,000$ $cm^2V^{-1}s^{-1}$ at 4.2 K, suggesting that $SrTiO_3$ may be an important component in oxide-based electronic devices. Some possibilities for such use have been demonstrated already in its use both as a gate and a channel in field effect transistors. For any future applications of electron-doped $SrTiO_3$, it is important to elucidate the stability of its electrical properties over time. For this reason, in this work we focus on relaxation effects of electrical transport in electron-doped $SrTiO_3$.

1.2 Fermi liquid

J. J. Thomson's discovery of the electron in 1897 had a vast and immediate impact on theories of the structure of matter. Three years after Thomson's discovery Drude constructed his theory of electrical and thermal conduction by applying the theory of gases to metals, considered as a gas of electrons.

In Drude's time it seemed reasonable to assume that the electronic velocity distribution, like that of an ordinary classical gas, was given in equilibrium by Maxwell-Boltzmann distribution:

$$f(\mathbf{v}) = n(\frac{m}{2\pi k_B T})^{3/2} e^{-mv^2/2k_B T} \tag{1.2}$$

Although Maxwell-Boltzmann distribution in conjunction with the Drude model successfully describe some of the physical properties of metals, there were two key problems: this model predicts that each electron should contribute $3k_B/2$ to the heat capacity of a metal - far from what was actually seen experimentally. In addition, the magnetic susceptibility did not show the Curie temperature dependence for free magnetic moments: $\chi \sim 1/T$.

This paradox cast a shadow over the the Drude model, which was only removed by the advent of the quantum theory and the recognition that for electrons the Pauli exclusion principle requires the replacement of the Maxwell-Boltzmann distribution (Eq. 1.2) with the Fermi-Dirac distribution:

$$f(\mathbf{v}) = \frac{(m/\hbar)^3}{4\pi^3} \frac{1}{e^{[(\frac{1}{2}mv^2 - k_B T_0)/k_B T]} + 1} \tag{1.3}$$

But then a new paradox appeared. Why should a theory based on non-interacting particles work so well in these systems where the energy scales of the kinetic energy

and Coulomb interaction are comparable. This paradox was resolved by Landau theory of Fermi liquids (FL) [18, 19, 20].

The basic assumption of Landau's theory is that the weakly excited states of a FL greatly resemble those of a weakly excited Fermi gas. These states can be described with a set of elementary excitations (quasi-particle) with spin $\frac{1}{2}$ and a momenta close to the Fermi surface. It is then assumed that there is one to one correspondence of the low energy eigenstates of the interacting electrons with those of the non-interacting Fermi gas. This may be physically realized by adiabatically switching on the interaction. We therefore retain the picture of Fermi particles and holes excitations carrying the same quantum numbers as their electron counter-parts in the free Fermi gas.

The FL model predicts certain temperature dependence at sufficiently low temperatures for physically observable quantities.[2] For example the heat capacity

$$c_v = \frac{1}{3}\frac{m^* p_F}{\hbar^3} k_B^2 T \tag{1.4}$$

and the magnetic susceptibility

$$\chi = \frac{\mu_B^2 m^* p_F}{\pi^2 \hbar^3 (1 + \overline{G})} \tag{1.5}$$

These are similar to the free Fermi gas results, except for the modified mass (m^*) and the $\overline{G}$ term in χ, which is related to the Landau $\mathfrak{f}$ function.[3] In addition, the resistivity

[2] In general, the physically observable quantities do not depend only on the "free" electrons contribution. The heat capacity for example has other contributions like phonons; In more general case $c_v = \gamma T + \beta T^3$ where γ is the electronic heat capacity constant and β is the phonon heat capacity constant.

[3] The total energy E of the liquid is not simply the sum of the energies of the quasi-particles. The quasi-particles's energy also depends on the distribution of other quasi-particles which Landau included via the '$\mathfrak{f}$ function', so the energy of the quasi-particles near the surface of the Fermi sphere is given by $\varepsilon(\mathbf{p}) = \varepsilon_F + v_F(p - p_F) + tr' \int \mathfrak{f}(\mathbf{p}, \mathbf{p}')\delta n(\mathbf{p}')d\tau'$.

has a $\rho = \rho_0 + A\rho^2$ dependence and the alternating current (AC) conductivity obeys the Drude form, $\sigma(\omega) = \sigma(0)/(1 - i\omega\tau)$.

FL is a remarkably successful theory that describes many metals including some where the interactions between the electrons are very strong. The heavy fermion problem provides an extreme example of the domain of validity of the Landau approach.

1.3 Non-Fermi liquid

1.3.1 General

Although metals that deviate from FL behavior were known for decades, only from March 1991, at the American Physical Society meeting, this issue generated a great deal of interest, including significant theoretical effort. At this meeting Seaman *et al.* presented measurements of heat capacity, magnetic susceptibility, and electrical resistivity of $Y_{1-x}U_xPd_3$ that clearly disagreed with the FL theory [21]. The theories that try to explain the NFL behavior can be divided into four categories: metals close to a quantum critical point, multichannel Kondo model, disordered Kondo models, and the Luttinger liquid.

Metals close to a quantum critical point

Quantum critical point (QCP) is a phase transition that occurs at zero temperature. FL theory breaks down near the fluctuations of a QCP. While at a finite temperature phase transition, the fluctuations that develop at a critical point are governed by classical physics and are limited to a narrow region around the phase transition. At a QCP, the critical fluctuations are quantum mechanical in nature and are felt over a wide range of temperatures above the quantum critical point, so the effect of quantum criticality is felt without ever reaching absolute zero.

The most common route to observe a QCP is by taking a system with a finite temperature phase transition and tuning it to $T = 0$, for example by applying pressure or magnetic field or changing its chemical composition (Fig. 1.3). MnSi is such an example, Fig. 1.4 shows that the ferromagnetic transition can be tuned to zero temperature by applying a pressure of ≈ 14.8 kbar [22, 23]. This value of the pressure indicates the QCP. $U_xY_{1-x}Pd_3$ [24] and $CeCu_{6-x}Au_x$ [25] are examples of tuning the anti-ferromagnetic transition to zero by doping.

Multichannel Kondo models

The simple Kondo model describes the behavior of a single spin-one-half magnetic ion interacting anti-ferromagnetically with a non-interacting sea of electrons. Passing electrons scatter from the impurity ion and both can exchange their spin directions. Kondo showed that in contrast to most electron scattering in metals which increase with increasing temperature this scattering decreases [26].

Nozières and Blandin developed the multichannel Kondo model for a single impurity [27]. In the multichannel case, the impurity ion intercats anti-ferromagnetically

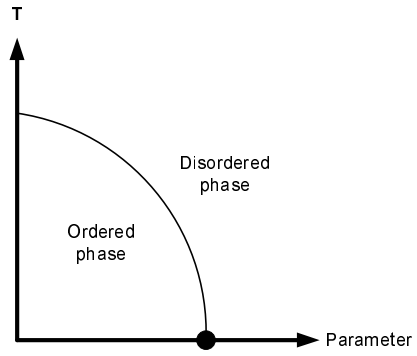

Figure 1.3: A qualitative phase diagram for a QCP. The QCP indicated by the black dot on the parameter axis. The parameter can be like pressure or magnetic field or chemical composition.

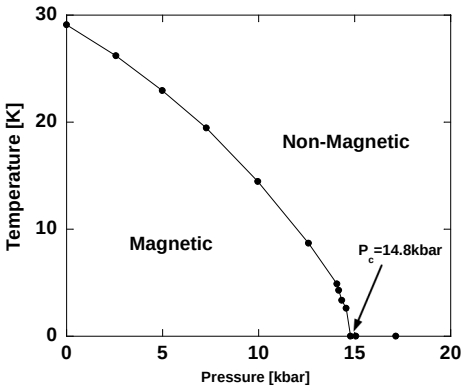

Figure 1.4: Magnetic phase diagram as a function of pressure of MnSi (from Ref. [23]).

with some seas of electrons (channels). The electrons are totally oblivious of the other seas, only the impurity sees that there is more than one channel. This model is described by the following Hamiltonian:

$$H = \sum_{k,m,\sigma} \varepsilon_k a^t_{km\sigma} a_{km\sigma} + J \sum_{k,k',m,\sigma,\sigma'} \mathbf{S} \cdot a^t_{km\sigma} \sigma_{\sigma\sigma'} a_{k'm\sigma'} \tag{1.6}$$

where $\mathbf{S}$ are the spin operators of the magnetic ion impurity, J is the antiferromagnetic interaction, σ are the Pauli matrices, and m labels the electrons channels. We can distinguish between three cases: (1) $n = 2S$, the number of channels is just sufficient to compensate the impurity spin to form a singlet. If $S = \frac{1}{2}$ and $n = 1$ it is the simple Kondo model. (2) $n < 2S$, there are not enough channels to compensate the impurity spin. (3) $n > 2S$, the impurity spin is overcompensated and generates a NFL behavior.

Disordered Kondo models

This model is based on the simple Kondo model in disordered systems. If the disorder creates a distribution of Kondo temperature,[4] this will lead to NFL behavior [28]. One such example is $UCu_{5-x}Pd_x$ [29].

Luttinger liquids

In one dimensional metals, the appearance of spin charge separation creates new quasi-particles instead of the Landau quasi-particles. The electron dissolves into its spin part (spinon) and its charge part (holon). It is clearly not a FL any more because the good quantum numbers look nothing like the old fermions quasi-particles labels.

[4]The Kondo temperature is the temperature in the simple Kondo model below which the impurity ion compensated.

1.3.2 Non-Fermi liquid behavior in ruthenates

Recently, ruthenates have attracted much attention as another class of materials that exhibits NFL behavior [3, 4, 5]. The ruthenates belong to $4d$ transition metal oxides, and the electron-electron correlation plays an important role in determining their physical properties. Although the NFL behavior in the ruthenates has been widely investigated, its origin is not clearly understood.

$CaRuO_3$ is a paramagnetic metal and since its low temperature resistivity is described by $\rho = \rho_0 + AT^\alpha$ with $\alpha \sim 1.5$, it is also considered a NFL metal [30]. This form of NFL resistivity is theoretically expected when there is a paramagnetic-to-antiferromagnetic QCP. We found that the low-temperature NFL behavior of $CaRuO_3$ is suppressed by magnetic field and is most effectively suppressed when a magnetic field is applied along the easy axis (EA) of magnetization, suggesting that critical spin fluctuations, possibly due to proximity of QCP, are related to the NFL behavior. The transport and thermodynamic properties of $SrRuO_3$ are also quite anomalous and exhibit a NFL behavior: the high temperature resistivity crosses the Ioffe-Regel limit [31], the temperature derivative of the magnetic-related resistivity near T_c strongly deviates from the expected heat capacity behavior. In addition, terahertz conductivity and infrared conductivity show non-Drude behavior [32, 33].

1.4 Hall effect (HE)

1.4.1 Ordinary Hall effect (OHE)

When a sample is placed in a magnetic field **B** and a current density **J** is passed through it, a transverse electric field $\mathbf{E}_{OHE}$ is set up and given by

$$\mathbf{E}_{OHE} = -R_0 \mathbf{J} \times \mathbf{B} \tag{1.7}$$

where R_0 is the ordinary Hall coefficient. The origin of the effect is the Lorentz force, $\mathbf{F} = q(\mathbf{E} + \mathbf{V} \times \mathbf{B})$, on the charge carriers in the magnetic field.

Using the most naive one band calculation

$$R_0 = \frac{1}{nq} \tag{1.8}$$

where n is the charge carrier density and q is their charge. As a result, the OHE is very useful as a means to measure the charge carrier density. One very important feature of the OHE is that it differentiates between positive charges moving in one direction and negative charges moving in the opposite direction. The OHE offered the first real proof that electric currents in metals are carried by moving electrons, not by protons. The OHE also showed that in some substances (especially P-type semiconductors), it is more appropriate to think of the current as positive "holes" moving rather than negative electrons. The OHE was widely used for these purposes in the current research.

1.4.2 Extraordinary Hall effect (EHE)

In magnetic materials the Hall effect includes, in addition to the OHE, an "extraordinary" Hall effect, which depends on the magnetization **M**. The EHE is usually

expressed as:

$$\mathbf{E}_{EHE} = -R_s \mathbf{J} \times \mu_0 \mathbf{M} \tag{1.9}$$

where R_s is the extraordinary Hall coefficient (this effect appears in addition to the contribution of $\mathbf{M}$ to the OHE according to the relation $B = H + 4\pi M$).

While the OHE is by now well understood, the understanding of the EHE is far from being complete despite considerable theoretical [34, 35, 36, 37] and experimental [38] efforts.

The common theoretical view is that

$$R_s = a\rho + b\rho^2 \tag{1.10}$$

where ρ is the longitudinal resistivity and a and b are constants. The linear term in ρ is attributed to asymmetric scattering ("skew scattering") of charge carriers, a process which derives from the classical Boltzmann equation [37]. On the other hand, the quadratic term in ρ is attributed to asymmetric side jumps which is a purely quantum scattering process [34]. This model, called "extrinsic" due to its dependence on scattering, is commonly used to describe EHE despite the existence of more than few cases in which it cannot fit the data [39]. More recently, a different model has been suggested [40, 41], called "intrinsic", which is correlated with Berry phase effect [42] in the crystal momentum space and it yields

$$\rho_{EHE} = -\rho^2 \sigma_{xy}^{BP}(M), \tag{1.11}$$

where the Berry phase transverse conductivity $\sigma_{xy}^{BP}(M)$ does not depend on ρ, and the dependence of σ_{xy}^{BP} on M can be calculated from the band structure.

The EHE in the itinerant ferromagnet $SrRuO_3$ poses a particular challenge. On the one hand, arguments in favor of a Berry phase model [43] have been contested [44]. On the other hand, the strict application of the extrinsic model has also been met with difficulties [45].

To obtain more insight on the EHE mechanism in this intriguing compound, we examine the EHE in $SrRuO_3$ in a different way. We study the EHE in the ultrathin limit, thus we increase the resistivity quite significantly without inducing structural disorder. On the one hand, our observation appears to be a strong confirmation of the extrinsic model which implies that R_s is a function of ρ alone. On the other hand, we see that above a certain temperature the EHE in $SrRuO_3$ is sensitive not only to the scattering rate but also to the nature of the scattering events. A similar possibility has been suggested in connection with the EHE exhibited by other materials [39, 46].

In addition, the EHE can be used to monitor the magnetization. It was widely used for this purpose in the current research, as will be explained in the manuscripts and in section 2.6.

1.5 Magnetoresistance

Magnetoresistance (MR) is the change of resistivity produced by a magnetic field and defined by

$$\mathrm{MR} = \frac{\rho(H) - \rho(0)}{\rho(0)} \tag{1.12}$$

In contrast to the OHE, in general the MR observed with H both parallel to or transverse to the current flow. Since the MR is an even function of the magnetic field, at low fields it is usually proportional to H^2. Various sources could contribute to the MR including:

Lorentz magnetoresistance- The deflection of the trajectories of the charge carriers due to Lorentz force increases the resistivity thus creating a positive MR. The longer the mean free path (lower resistivity) relative to cyclotron radius, the larger the effect of the field on the resistance.[5]

An ubiquitous behavior in Fermi liquid metals is the scaling of the MR by Kohler's rule which states that the MR is a function of $H\tau$ alone (where τ is the scattering time) [47]. In conventional metals $\rho \propto 1/\tau$, which results in a scaling law of the form $\Delta\rho/\rho = f(H/\rho)$. We used Kohler's rule to show that the scattering time, in Electron-doped $SrTiO_3$, is practically unchanged as a function of relaxation time or irradiation time.

Suppression of spin fluctuation- An external magnetic field suppresses spin fluctuations. Since spin fluctuations contribute to the resistivity, a magnetic field yields

[5]It seems that the Hall electric field counteracted the effect of the magnetic field in such a way at to leave the resistance unaltered. This was perfectly satisfactory for carriers with a single mobility, velocity and effective mass. However, if two types (or more) of carrier are presented, the Hall field will not able to buck out the effects of the magnetic field of both carriers. In this case the resistance is changed.

a negative MR.

Anisotropic Magnetoresistance- The dependence of the resistivity on the orientation of the magnetization with respect to the electric current direction in the material is known as Anisotropic Magnetoresistance (AMR). The discovery of the AMR was made by William Thomson in 1857.[6] However, the importance of the AMR was recognized more than a century later by using the AMR phenomenon in sensors for magnetic recording. The origin of the AMR stems from the anisotropy of scattering produced by spin-orbit coupling [48].

[6]Known as Lord Kelvin.

1.6 Strontium ruthenate ($SrRuO_3$)

1.6.1 General

In the last decades the ferromagnetic perovskite $SrRuO_3$ has attracted a great deal of attention. This attention is driven in part by scientific curiosity and in part by technological application. From the scientific curiosity point of view, one of the important open questions is the degree of electron-electron correlations and how correlations affect the physical properties of the material, which in part are abnormal and exhibit NFL behavior. The technological interest is related to the use of $SrRuO_3$ in future all oxide electronics device applications due to its chemical stability, metallic conductivity, and epitaxial growth on perovskite substrates.

While this compound is not likely to be relevant for spintronics applications due to its relatively low Curie temperature, it is a compound that allows the study of basic spintronics effects due to its special features. In particular, it has very high uniaxial magnetocrystalline anisotropy. These features make this compound an ideal model system for studying spin transport in the presence of magnetic interfaces.

1.6.2 Crystalline structure

$SrRuO_3$ belongs to the perovskite group. At room temperature $SrRuO_3$ exhibits an orthorhombic symmetry with lattice parameters 5.53 Å, 5.57 Å and 7.85 Å correspond to [100], [010], and [001],[7] respectively, and a slightly distorted pseudo-cubic unit cell (the thick solid line in Figure 1.5) with a lattice parameter of 3.93 Å.

The crystalline orientation of the thin films of $SrRuO_3$ strongly depends on the

[7] In this work Miller indices based on the orthorhombic unit cell are used.

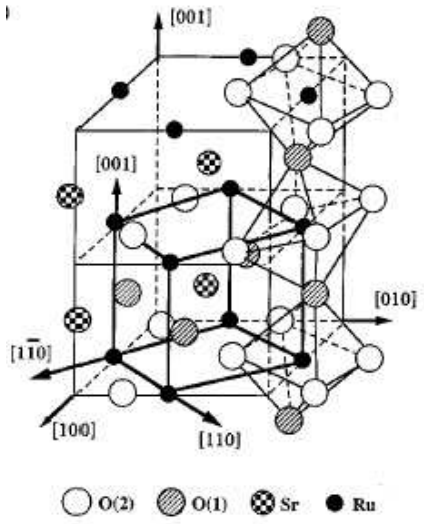

Figure 1.5: Schematic diagram of $SrRuO_3$ crystal structure in orthorhombic unit cell. The inner cube constructed by thick solid lines is the pseudo-cubic unit cell (picture from Ref. [50]).

substrate: On $SrTiO_3$ the films mostly grow with the [001] axis in the film plane [49], but some grains grow with the [001] axis perpendicular to the film plane. Much better films of $SrRuO_3$ can be grown on miscut $SrTiO_3$ substrates for which the [001] axis of the film lies perpendicular to the miscut direction.

In our experiments, we used epitaxial $SrRuO_3$ thin films grown on a slightly miscut (2^o) $SrTiO_3$ substrate. The films grown on such a substrate grow with the [001] direction in the plane of the film and the [010] direction at 45^o out of the film plane (for more details see section 2.1).

The strain, in epitaxial growth, further distorts the lattice structure of $SrRuO_3$. The substrate compress the lattice of the $SrRuO_3$ along [$\bar{1}$10] [001] and expands along [110] direction. This causes further tilting and rotating of the RuO_6 octahedra in thin films relative to the bulk [50].

1.6.3 Transport and thermodynamic properties

The transport and thermodynamic properties of $SrRuO_3$ are quite anomalous. Its electrical resistivity is relatively large ($\rho \sim 200$ $\mu\Omega$ cm at room temperature), and continues to grow as a function of temperature almost without saturation, and seems to cross the Ioffe-Regel limit [31]. Furthermore, terahertz conductivity and infrared conductivity show non-Drude behavior [32, 33].

In addition, the behavior of the temperature derivative of the resistivity near T_c strongly deviates from Fisher-Langer theory [51, 52], and the resistivity shows deviations from Matthiessen's rule [53, 54].

Despite these anomalies, which part of them strongly indicate NFL behavior, the resistivity at low temperature has a $\rho = \rho_0 + A\rho^2$ dependence [51, 52], the heat capacity obeys at low temperatures $c_v = \gamma T + \beta T^3$ [31], and quantum oscillations in the electrical resistivity at high magnetic fields (the Shubnikov-de Haas oscillations) show an existence of conventional fermion quasiparticles [55].

However, the coefficient, A, of the T^2 term in the resistivity is three order of magnitude larger than elemental ferromagnets values. The measured linear heat capacity coefficient, γ, is 30 mJ/mol K^2, which is larger than one would estimate for typical metal and exceeds the theoretical value, calculated from band calculations, by a factor of 3.7. These high values of γ and A are evidence of the strong electronic interactions.

1.6.4 Magnetic properties

$SrRuO_3$ is a ferromagnet with $T_c \sim 165$ K for bulk materials and ~ 150 K for films. Magnetism in $SrRuO_3$ is itinerant and it originates from the $4d$ electrons of the Ru atoms. The spontaneous magnetization in the zero-temperature limit in bulk (films) is 1.6 μ_B (1.4 μ_B), which is consistent with band calculations [31].

Magnetocrystalline anisotropy studies of bulk single crystals have shown that there are two magnetic EA along the face diagonals of the pseudo-cubic unit cell, which are the orthorhombic [100] and [010] directions (see Figure 1.5) [56]. In contrast to bulk, epitaxial thin films of $SrRuO_3$ are characterized by a single EA whose orientation is temperature dependent [50, 52]. Above T_c the EA coincides with [010] which is at 45^o relative to the film normal, while below T_c there is a reorientation transition where the EA rotates in the (001) plane approaching $\sim 30^o$ relative to the normal at 2 K [52]. The difference between the bulk and the thin films is probably a result of a further distortion of the already distorted bulk lattice by tilting and rotating the RuO_6 octahedra.

The Magnetocrystalline anisotropy energy can be described by $E = K \sin^2 \theta$, with a weakly temperature-dependent anisotropy constant, $K \sim 1.2 \times 10^7$ erg/cm^3. The large Magnetocrystalline anisotropy is mainly a result of the crystal distortion and the large spin-orbit coupling.

1.7 Calcium ruthenate ($CaRuO_3$)

1.7.1 General

$CaRuO_3$ is one of the most intriguing members of the ruthenate perovskites group. It is a metal with a $GdFeO_3$-type orthorhombic structure [57], and since its low-temperature resistivity is described by $\rho = \rho_0 + A\rho^{\alpha}$ with $\alpha \sim 1.5$, it is also considered a NFL metal. Despite the fact that it has been studied since the late 1950s, its magnetic properties have been quite elusive. Although the most acceptable view today is that $CaRuO_3$ is a paramagnetic metal [58, 59, 60], there were reports of antiferromagnetic ordering [61], of parasitic ferromagnetic phase [62] and also of spin-glass behavior [63].

1.7.2 Crystalline structure

The crystal structure of $CaRuO_3$ is the same as the crystal structure of $SrRuO_3$ having lattice parameters of 5.54 Å, 5.36 Å and 7.68 Å (see Figure 1.6)[57, 64]. $CaRuO_3$ is more distorted due to the rotation of the RuO_6 which is approximately twice as large as that observed for $SrRuO_3$, as expected, because the Ca ionic radius is even less ideal for perovskite formation than Sr.

1.7.3 Transport and thermodynamic properties

$CaRuO_3$ has attracted considerable interest due to its anomalous transport and thermodynamic properties:

Electrical conductivity - Its resistivity at high temperatures has a $T^{1/2}$ dependence crossing over to a $T^{3/2}$ dependence at low temperatures [30], suggesting an antiferromagnetic QCP. Additional abnormal properties of the conductivity include:

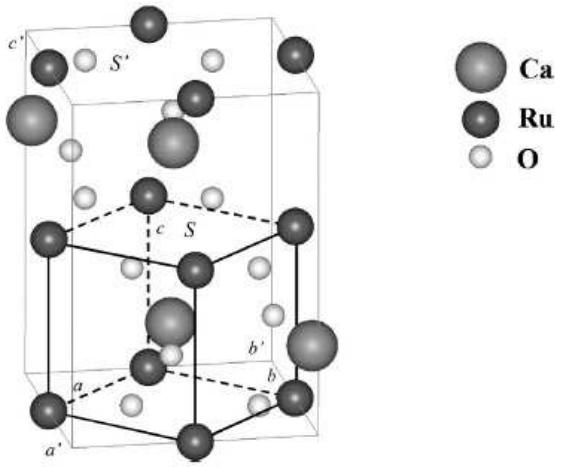

Figure 1.6: Schematic diagram of $CaRuO_3$ crystal structure in orthorhombic unit cell. The inner cube constructed by thick solid lines is the pseudo-cubic unit cell (picture from Ref. [64]).

non-Drude behavior of the optical conductivity, which shows a NFL behavior of $\sigma_1(\omega) \sim 1/\omega^{1/2}$, in contrast to the usual Drude form of $1/\omega^2$ [65], and negative deviations from Mattiessens's rule [53].

Heat capacity - Heat capacity measurements for $1.5 < T < 10$ K show that $c_v = \gamma T + \beta T^3$ and its γ value ($\sim$ 70 mJ/mol K^2) is larger than the γ value in $SrRuO_3$ ($\sim$ 30 mJ/mol K^2), suggesting that electron-electron correlations in $CaRuO_3$ are even stronger than in $SrRuO_3$ [57]. On the other hand, Cao *et al.* showed that the heat capacity is proportional to $-Tlog(T)$ below 13 K, which is evidently a NFL behavior[66].

Shubnikov-de Haas oscillations - No Shubnikov-de Haas oscillations are observed down to T=0.65 K for applied magnetic fields up to 45 T [66]. The absence of the Shubnikov-de Haas oscillations is not surprising since the quasi-particles are not well defined near a QCP.

1.7.4 Magnetic properties

Magnetic susceptibility - For high temperatures the susceptibility obeys the modified Curie-Weiss law: $\chi(T) = \chi_0 + C/(T - \Theta)$ with a high positive value of χ_0 [56, 57]. Because χ_0 represents Pauli paramagnetism (Eq. 1.5), Landau diamagnetism and core diamagnetism the high positive value indicates strong electron-electron correlations. At low temperatures the susceptibility obeys T^{γ} with $0.5 < \gamma < 1$, depending on the applied magnetic field [66]. The high sensitivity of the temperature exponent to magnetic fields suggests a proximity to a magnetic instability. Similar behavior has been observed in other QCP systems like $SrIrO_3$ [67].

Magnetic ground state - Despite the fact that $CaRuO_3$ has been studied since the late 1950s, its magnetic properties have been quite elusive. In addition to reports indicating that $CaRuO_3$ is a paramagnetic metal [58, 59, 60], there were reports of antiferromagnetic ordering with $T_N \sim 110$ K [61], of parasitic ferromagnetic phase [62], and also of spin-glass behavior [63]. On the other hand, recent reports suggest that $CaRuO_3$ is paramagnetic in the sense that there is no magnetic order or magnetic hysteresis; however, it is a nearly ferromagnetic metal [68, 69]; namely, it is affected by enhanced ferromagnetic fluctuations. He and Cava [70] found that substitution of as little as 2% of Ru by Ti induces ferromagnetism in $CaRuO_3$. This finding could suggest that ferromagnetic behavior in $CaRuO_3$ is non-intrinsic; however, other sources such as minor lattice distortions cannot be excluded. Our samples are untwinned films grown either on $SrTiO_3$ or on $NaGaO_3$ that show no magnetic hysteresis down to at least 2 K.

A possible origin for this unusual state of conflicting reports could be the prox-

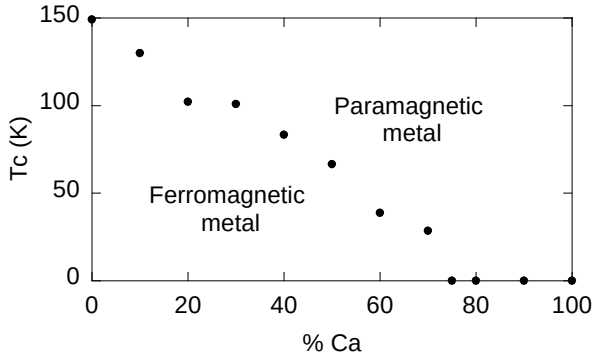

Figure 1.7: Ferromagnetic phase diagram of $Ca_xSr_{1-x}RuO_3$ (picture from Ref. [71]).

imity of $CaRuO_3$ to a magnetic QCP. The perovskite $Ca_xSr_{1-x}RuO_3$ series is a good candidate system for observing NFL behavior at the vicinity of a ferromagnetic QCP, given that $SrRuO_3$ is a ferromagnet whose T_c can be completely suppressed via Ca doping (see Fig. 1.7)[71]. Such proximity to QCP could explain the extreme sensitivity of the magnetic ground state to small changes either in crystal structure or doping. In addition, it can also be the source of the NFL behavior.

1.8 Strontium titanate ($SrTiO_3$)

1.8.1 General

Strontium titanate is a wide-band gap ($E_g \sim 3.2$ eV) semiconductor (band insulator) [72, 73] with a perovskite crystal structure. $SrTiO_3$ attracts considerable interest for its unique dielectric properties, i.e., its very large dielectric constant [74, 75] and nonlinear behavior when an electric field is applied [76]. In contrast to $CaRuO_3$ and $SrRuO_3$, at room temperature $SrTiO_3$ exists in the cubic form, but transforms into tetragonal structure at temperatures less than 105 K. $SrTiO_3$ is the prototypical substrate type for the thin film growth of perovskites, and as such is widely used by materials scientists and physicists alike.

In addition to serving as a substrate for perovskite films, $SrTiO_3$ may be used to produce high mobility conductors that would be useful in future oxide electronics.

1.8.2 Electron-doped $SrTiO_3$

In addition to being considered by many the ideal insulating substrate on which epitaxial films of perovskites are grown, now it seems that electron-doped $SrTiO_3$ may also play an important role. Recent excitement in the field is related to reports on the formation of a quasi two dimensional electron gas at $SrTiO_3 - LaAlO_3$ interface with mobilities on the order of $10,000$ $cm^2V^{-1}s^{-1}$ at 4.2 K [77, 78, 79]. On the other hand, other reports claim that this is not an interface effect but a conduction of electron-doped $SrTiO_3$ formed due to oxygen vacancies in $SrTiO_3$ [80, 81, 82]. Irrespective of the dispute regarding the source of high mobility in $SrTiO_3 - LaAlO_3$ systems, it is clear that the electron gas in oxygen deficient $SrTiO_3$ exhibits similar mobilities

which might make it an important component for spintronics with perovskites. The use of $SrTiO_{3-\delta}$ in electronic devices has been demonstrated already in its use as a gate [83] and a channel [84, 85] in field effect transistors. Electron doping $SrTiO_3$ by creating oxygen vacancies (which transforms $SrTiO_3$ into $SrTiO_{3-\delta}$) can be achieved in various ways including high-temperature annealing in oxygen reduced pressure and Ar^+-irradiation [86, 87, 88, 89]. Recently, there have been new reports on the use of Ar^+-irradiation for obtaining highly conductive $SrTiO_3$ [90, 91] including the detection of blue light emission from Ar^+-irradiated $SrTiO_3$ [91].

Our $SrTiO_3$ samples were irradiated with Ar^+ ions. We found with our samples that they become conducting when the irradiation time exceeds 30 s, the mobility is similar in its magnitude and its temperature dependence to other systems with electron doped $SrTiO_3$ and the residual resistivity ratio (RRR) exceeds 500. Similar and even higher values of RRR have been reported for electron doped $SrTiO_3$ and $SrTiO_3 - LaAlO_3$ heterostructures.

Chapter 2

Experimental Details

2.1 Sample fabrication

2.1.1 $SrRuO_3$

Efforts to grow thin films of $SrRuO_3$ on different substrates have been made. Films on $LaAlO_3$/[001] substrates are orthorhombic with the [001]-axis mainly lying in the plane of the film (along either of the two principal directions); however, there is also a varying component of [001]-perpendicular grains. The dense twinning of $LaAlO_3$ substrates is probably responsible for the relatively poor quality of these films.

Thin films of $SrRuO_3$ that grown on $SrTiO_3$ substrates are much better. Although they mostly grow with the [001]-axis in the film plane (again along either of the two principal directions) [49], some [001]-perpendicular grain have been observed (up to 20 percent). Even better films can be grown on miscut $SrTiO_3$ substrates for which the [001]-axis of the film lies perpendicular to the miscut direction (see Figure 2.1).

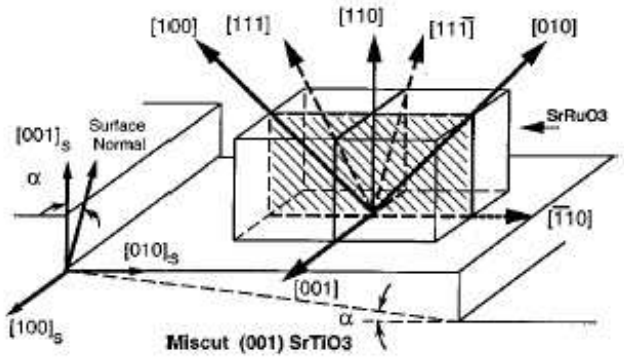

Figure 2.1: The lattice orientation of $SrRuO_3$ (110) films on miscut (001) $SrTiO_3$ substrate (picture from Ref. [50]).

Our samples were grown by J. W. Reiner at Stanford University in the laboratory of M. R. Beasley. The samples are epitaxial thin films grown on slightly miscut ($\sim 2^o$) substrates of $SrTiO_3$ by reactive electron beam evaporation. Growth rates were measured by an *in-situ* quartz microbalance. These growth rates were calibrated against finite thickness oscillations observed in x-ray diffraction (XRD) studies of 50-100 nm films [92]. These XRD studies also demonstrated that the $SrRuO_3$ films are untwinned orthorhombic single-crystals, with lattice parameters of $a \cong 5.53$ $\mathring{A}$, $b \cong 5.57$ $\mathring{A}$ and $c \cong 7.85$ $\mathring{A}$. The [001] direction is in the plane of the film and the [010] direction is at 45^o out of the film plane.

2.1.2 $CaRuO_3$

Although $CaRuO_3$ has many similarities to $SrRuO_3$ (as shown in section 1.7), the lattice mismatch between $CaRuO_3$ and $SrTiO_3$ is three times as large as for $SrRuO_3$ and it is much harder to grow an untwinned $CaRuO_3$ than $SrRuO_3$.

Our $CaRuO_3$ samples were also grown by J. W. Reiner at Stanford University in the laboratory of M. R. Beasley. The samples grown either on $SrTiO_3$ or on

$NaGaO_3$ (both regular and miscut) by molecular beam epitaxy. The films grown on the $NaGaO_3$ are better than the films grown on $SrTiO_3$. X-ray scans, of $CaRuO_3$ grown on $NaGaO_3$, show single $CaRuO_3$ phase and a rocking curve with full-width half-maximum of 0.051^o [92].

2.1.3 Electron-doped $SrTiO_3$

Our samples are commercially available[1] one sided polished $SrTiO_3$ crystals ($5 \times 5 \times 0.5$ mm^3). As mentioned above, one of the methods to dope $SrTiO_3$ with electrons is by Ar^+ irradiation. We found in our group that irradiating $SrTiO_3$ substrates for one minute with Ar^+ ions accelerated at 4 kV and fluence on the order of 10^{15} ions per second per cm^2 is sufficient for obtaining high mobility $SrTiO_{3-\delta}$ with a charge carrier sheet density of $\approx 10^{14}$ cm^{-2} of electrons and no more changes in conductivity are observed after several minutes of irradiation.[2] We note that this process is reversible and by heating the sample in a rich oxygen environment the sample returns to be an insulator.

The estimated penetration depth of the ions, L, in Å is given by the empirical formula [90, 93] $L = 1.1 \times \frac{E^{2/3} \times W}{\rho \times (Z_i^{1/4} + Z_t^{1/4})^2}$ where E is the energy in eV, W is the atomic weight of the target in atomic mass units, ρ is the target density, and Z_i, Z_t are the atomic numbers of the ions and the target, respectively (since $SrTiO_3$ is a compound, we use for the target the weighted average of the atomic weights and numbers). In our case $L \approx 120$ Å; therefore, we expect that the thickness of the conducting layer will be on this order. Using the estimated penetration depth, we estimated that the

[1] TBL-Kelpin company.

[2] Since the thickness of the conducting layer is unknown we can find from the OHE only the sheet density.

charge carrier density is $\approx 10^{20}$ cm^{-3}.

2.2 Sample preparation

2.2.1 $SrRuO_3$ and $CaRuO_3$

We patterned the films by conventional Photolithography to allow precise measurements of longitudinal and transverse resistivity. A typical pattern scheme is shown in Figure 2.2.

Photolithography is the process of using light to create a pattern: First we coated the film with a polymer which is sensitive to ultraviolet light, called a photoresist (see Figure 2.3(a)). Ultraviolet light is then shone through a mask onto the photoresist (Figure 2.3(b)). The photoresist is developed, a process which transfers the pattern on the mask to the photoresist layer (Figure 2.3(c)).

There are two types of photoresist, termed positive and negative. Where the ultraviolet light strikes the positive resist it weakens the polymer, so that when the image is developed the resist is washed away where the light struck it - transferring a positive image of the mask to the resist layer. The opposite occurs with negative resist. Where the ultraviolet light strikes negative resist it strengthens the polymer, so by developing, the unexposed resist washed away - a negative image of the mask is transferred to the resist.

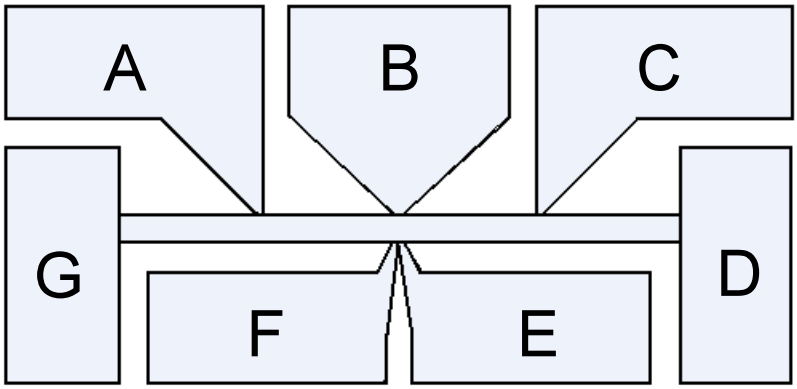

Figure 2.2: A typical pattern for measurement of longitudinal and transverse resistivity. The length and the width of the current path are 1 mm and 50 μm, respectively.

Argon ion milling is then used to remove the film where it is exposed through the openings in the resist. Finally the resist is removed by Acetone leaving the patterned film (Figure 2.3(d)).

2.2.2 Electron-doped $SrTiO_3$

To irradiate only specific parts of the substrates in shapes that will allow resistivity and Hall measurement, we have used conventional photolithography that left photoresist on the samples except for windows in the desired shapes.

2.3 Equipment

In this research we used the following Equipment:

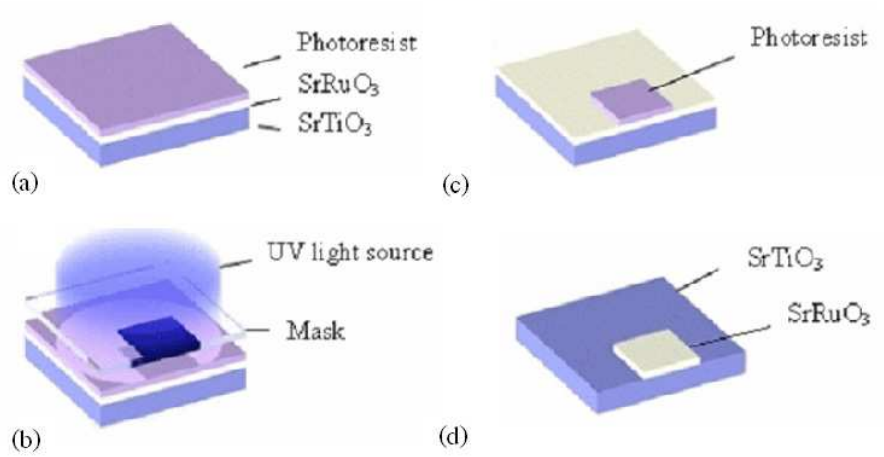

Figure 2.3: The Photolithography Process

- A Quantum Design Physical Properties Measuring System (PPMS) with the following specifications: Temperature range: 1.8 K - 400 K with ^{4}He, extended down to 0.35 K when the ^{3}He insert is used. Field range is 9 T. Measurements: transport and magnetotransport measurements (DC,AC) with rotation in a field (down to 1.8 K), AC DC magnetometer (down to 1.8 K), magnetic torque (down to 1.8 K), heat capacity (down to 0.35 K).

- A Superconducting Quantum Interference Device (SQUID) by Quantum Design for measuring magnetic moments parallel and perpendicular to the applied magnetic field down to $1 \cdot 10^{-9}$ emu, which has the following capabilities: Temperature range: from 1.7 K up to 400 K; magnetic fields: up to 7 T. Rotator: allows to rotate the sample relative to the magnetic field in the plane of the film and in planes perpendicular to the film plane.

- A Precision Etching Coating System (PECS) manufactured by Gatan which is used for etching samples that underwent photolithography and for sputtering.

- A west-Bond wire bonder.
- A clean room with photolithography facilities.
- High Resolution Scanning Electron Microscope - In addition to scanning possibilities, the system is equipped with (a) Raith-50 e-beam Lithography system which allows patterning with resolution below 10 nm, and (b) EDS for compositional analysis.

2.4 Measuring technique

In measuring the OHE and EHE certain associated effects give rise to potentials which must be corrected in order to avoid error in the measured value. The largest effect is the resistance, which appears because of the experimental difficulty in aligning the measuring voltage probes. Another important effect is the planar Hall effect (PHE)[3]. However, since the longitudinal contribution and the PHE contribution remain the same when the direction of **B** and **M** are reversed while the EHE and OHE are antisymmetric under magnetization reversal and under magnetic field reversal, respectively, the HE resistance measured between the pads marked B and E (see Figure

[3]The planar Hall effect is the appearance of transverse resistivity, ρ_{xy}, which arises whenever there is resistivity anisotropy and the current is not along one of the principal axes of the resistivity tensor.

2.2) can be determined as:

$$R_{OHE}(B,M) + R_{EHE}(B,M) = \frac{R_{GD,BE}(B,M) - R_{GD,BE}(-B,-M)}{2} \tag{2.1}$$

Here the first pair of indices represents the contact used to supply and draw current, and the second pair of indices represents the probes used to measure the potential difference.

The reciprocity theorem asserts that in the presence of a magnetic field the exchange of the current and voltage leads has to be accompanied by a reversal of the magnetic field and magnetization [94, 95]

$$R_{GD,BE}(B,M) = R_{BE,GD}(-B,-M). \tag{2.2}$$

So according to this relation Eq. 2.1 can be written as:

$$R_{OHE}(B,M) + R_{EHE}(B,M) = \frac{R_{GD,BE}(B,M) - R_{BE,GD}(B,M)}{2} \tag{2.3}$$

which is much more simple measurement.

Another problematic contribution which affects both the longitudinal and the transverse measurements is the contact resistance. In order to exclude this contribution we used the fact that the contact resistance, Δ, does not depend on the direction of the current and $R_{BE,GD} = -R_{EB,GD}$ so

$$R_{BE,GD} = \frac{\tilde{R}_{BE,GD} - \tilde{R}_{EB,GD}}{2} = \frac{(R_{BE,GD} + \Delta) - (R_{EB,GD} + \Delta)}{2}. \tag{2.4}$$

2.5 Identification of the OHE and the EHE

In order to separate, in $SrRuO_3$, the OHE contribution from the EHE we measured the HE at a low magnetic field ($H \leq 0.4$ T) as a function of the direction of the field.[4] In such fields, the change in ρ_{xy} is linear in H. In addition, for such fields $\mathbf{M}$ does not rotate away from the EA (because the anisotropy field is of order of 10 T). If the easy axis is not perpendicular to film surface, the EHE and the OHE contributions have different symmetries, and can be separated. The behavior can be fitted as a sum of the OHE and the EHE contributions according to the formula

$$\Delta\rho_{xy} = R_0 H \cos\alpha + \frac{d\rho_{xy}^{EHE}}{dM}\chi H \cos(\alpha - \alpha_{ea}), \tag{2.5}$$

where α_{ea} is the direction of the easy axis, α is the direction of the magnetic field - both are measured from an axis perpendicular to the film surface - and χ is the magnetic susceptibility.

We used two important properties of $SrRuO_3$ to allow minimal uncertainty in the identification of the zero field EHE below T_C. First after fully aligning the magnetization of the sample by field cooling, there is no nucleation of reversed magnetization regions when the field is set to zero. Therefore, in a remnant state we measure the full contribution of the spontaneous magnetization to the HE. Second, the self field created by the remnant magnetization induces a small OHE whose contribution to the total HE at zero applied field can be generally neglected. As a result of these two properties we may reliably identify the zero field HE with the EHE.

[4] Here and in the next section we described only the methods of $SrRuO_3$. Since $CaRuO_3$ is paramagnetic the situation is much more complicated and we described it in our articles.

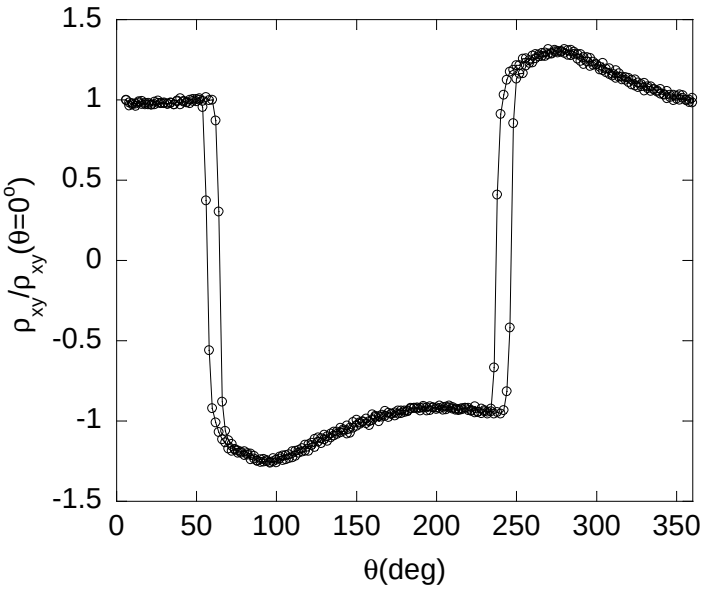

Figure 2.4: Hall effect of a single-orientation film (3.9 nm) as a function of the magnetic field direction (θ is measured relative to the normal to the film, in the (001) plane) at $T = 125$ K, $H = 1$ T (the two curves correspond to sweeps clockwise and anticlockwise in the angle).

2.6 Sample characterization

To determine the magnetic anisotropy of ultrathin films of $SrRuO_3$, we have used both magnetization and magneto-transport measurements. The magnetization measurements were performed with a Quantum Design SQUID magnetometer capable of measuring longitudinal and transverse magnetic moments. The sample was cooled in a field down to 2 K where the field was turned off. Afterwards, both the transverse and longitudinal moments were measured as a function of temperature between 2 K and T_c. Due to the low signal (particularly in the thinnest films), complementary magnetotransport measurements were performed - particularly, EHE measurements.

To find the EA direction, we rotate the sample in the (001) plane forwards and

backwards relative to an applied magnetic field. As the field is rotated away from the EA, the magnetization also deviates from the EA, but it does not follow the field because of the large magnetic anisotropy. When the angle between the field and the EA exceeds 90^o, the magnetization abruptly reverses its orientation, which yields jumps in the Hall resistivity (see Figure 2.4). Based on symmetry consideration the EA is 90^o away from the average angle obtained in clockwise and anticlockwise rotations.

We used this method to ensure that the measured samples were not composed of grains with different crystallographic orientations. In samples which involve a mixture of several orientations, jumps occur at additional angles, corresponding to configurations with different orientations of the EA.

Chapter 3

Manuscripts

Magnetic and transport properties of epitaxial films of $SrRuO_3$ in the ultrathin limit
M. Schultz, James W. Reiner, and L. Klein (submitted to Phys. Rev. B).

The extraordinary Hall effect of $SrRuO_3$ in the ultrathin limit
M. Schultz, James W. Reiner, and L. Klein (accepted for publication in J. Appl. Phys.).

Uniaxial magnetocrystalline anisotropy in $CaRuO_3$
M. Schultz, L. Klein, J. W. Reiner, and M. R. Beasley, Phys. Rev. B **73**, 085109 (2006).

Low-temperature magnetoresistance in untwinned $CaRuO_3$ films
M. Schultz, L. Klein, J. W. Reiner, and M. R. Beasley, Physica B **378-380**, 490 (2006).

Relaxation of transport properties in electron-doped $SrTiO_3$
M. Schultz, and L. Klein, Appl. Phys. Lett. **91**,151104 (2007).

a

3.1 Magnetic and transport properties of epitaxial films of $SrRuO_3$ in the ultrathin limit

a

a

a

a

a

3.2 The extraordinary Hall effect of $SrRuO_3$ in the ultrathin limit

a

a

a

3.3 Uniaxial magnetocrystalline anisotropy in $CaRuO_3$

a

a

a

3.4 Low-temperature magnetoresistance in untwinned $CaRuO_3$ films

a

3.5 Relaxation of transport properties in electron-doped $SrTiO_3$

a

a

a

Bibliography

[1] J. G. Bednorz, and K. A. Müller, Z. Phys. B **64**, 189 (1986).

[2] R. von Helmolt, J. Wecker, B. Holzapfel, L. Schultz, and K. Samwer, Phys. Rev. Lett. **71**, 2331 (1993).

[3] P. Khalifah, K. D. Nelson, R. Jin, Z. Q. Mao, Y. Liu, Q. Huang, X. P. A. Gao, A. P. Ramirez, and R. J. Cava1, Nature **411**, 669 (2001).

[4] J. Alloys and Comp **383**, 313 (2004).

[5] S. A. Grigera, R. S. Perry, A. J. Schofield , M. Chia, S. R. Julian, G. G. Lonzarich, S. I. Ikeda, Y. Maeno, A. J. Millis, and A. P. Mackenzie, Science **294**, 329 (2001).

[6] G. A. Prinz, Science **282**, 1660 (1998).

[7] S. A. Wolf, D. D. Awschalom, R. A. Buhrman, J. M. Daughton, S. von Molnár, M. L. Roukes, A. Y. Chtchelkanova, and D. M. Treger, science **294**, 1488 (2001).

[8] I. Žutić, J. Fabian, and S. Das Sarma, Rev. Mod. Phys. **76**, 323 (2004).

[9] S. A. Wolf, A. Y. Chtchelkanova, and D. M. Treger, IBM J. Res. and Dev. **50**, 101 (2006).

[10] M. N. Baibich, J. M. Broto, A. Fert, F. Nguyen Van Dau, F. Petroff, P. Eitenne, G. Creuzet, A. Friederich, and J. Chazelas, Phys. Rev. Lett. **61**, 2472 (1988).

[11] J. S. Moodera, Lisa R. Kinder, Terrilyn M. Wong, and R. Meservey, Phys. Rev. Lett. **74**, 3273. (1995).

[12] G. Schmidt, D. Ferrand, and L. W. Molenkamp, A. T. Filip and B. J. van Wees, Phys. Rev. B **62**, R4790 (2000).

[13] M. Gajek, M. Bibes, A. Barthélémy, K. Bouzehouane, S. Fusil, M. Varela, J. Fontcuberta, and A. Fert, Phys. Rev. B **72**, 020406(R) (2005).

[14] G. Herranz, M. Basletic, M. Bibes, R. Ranchal, A. Hamzic, E. Tafra, K. Bouzehouane, E. Jacquet, J. P. Contour, A. Barthélémy, and A. Fert, Phys. Rev. B **73**, 064403 (2006).

[15] G. Herranz, R. Ranchal, M. Bibes, H. Jaffrès, E. Jacquet, J.-L. Maurice, K. Bouzehouane, F. Wyczisk, E. Tafra, M. Basletic, A. Hamzic, C. Colliex, J. P. Contour, A. Barthélémy, and A. Fert, Phys. Rev. Lett. **96**, 027207 (2006).

[16] M. Feigenson, J. W. Reiner, and L. Klein, Phys. Rev. Lett. **98**, 247204 (2007).

[17] L. Klein,Y. Kats, A. F. Marshall, J. W. Reiner, T. H. Geballe, M. R. Beasley, A. Kapitulnik, Phys. Rev. Lett. **84**, 6090 (2000).

[18] L. D. Landau, Sov. Phys. JETP **3**, 920 (1957).

[19] L. D. Landau, Sov. Phys. JETP **5**, 101 (1957).

[20] L. D. Landau, Sov. Phys. JETP **8**, 70 (1959).

[21] C. L. Seaman, M. B. Maple, B. W. Lee, S. Ghamaty, M. S. Torikachvili, J. -S. Kang, L. Z. Liu, J. W. Allen, and D. L. Cox, Phys. Rev. Lett. **67**, 2882 (1991).

[22] C. Pfleiderer, G. J. McMullan, S. R. Julian, and G. G. Lonzarich, Phys. Rev. B **55**, 8330 (1997).

[23] C. Thessieu, J. Floquet, G. Lapertot, A. N. Stepanov, and D. Jaccard, Solid State Comm. **95**, 707 (1995).

[24] C. L. Seamam, M. B. Maple, B. W. Lee, S. Ghamaty, M. S. Torikachvil, J. S. Kang,L.Z. Liu, J. W. Allen, and D. L. Cox, Phys. Rev. Lett. **67**, 2882 (1991).

[25] H. von Lohneysen, J. Phys.: Condense. Matter. **8**, 9689 (1996).

[26] J. Kondo, Prog. Theor. Phys. **32**, 37 (1964).

[27] P. Nozières , and A. Blandin, J. Phys. **41**, 193, (1980).

[28] E. Miranda, V. Dobrosavljevic, and G.Kotilar, Phys. Rev. Lett. **78**, 290 (1997).

[29] O. O. Bernal, D. E. Maclaughlin, H. G. Lukefahr, and B. Andraka, Phys. Rev. Lett. **75**, 2023 (1995).

[30] L. Klein, L. Antognazza, T. H. Geballe, M. R. Beasley, and A. Kapitulnik, Phys. Rev. B **60**, 1448 (1999).

[31] P. B. Allen, H. Berger, O. Chauvet, L. Fano, T. Jarlborg, A. Junod, B. Revaz and G. Santi, Phys. Rev. B **53**, 4393 (1996).

[32] P. Kostic, Y. Okada, N. C. Collins, Z. Schlesinger, J. R. Reiner, L. Klein, A. Kapitulnik, T. H. Geballe, and M. R. Beasley, Phys. Rev. Lett. **81**, 2498 (1998).

[33] J. S. Dodge, C. P. Weber, J. Corson, J. Orenstein, Z. Schlesinger, J. W. Reiner, and M. R. Beasley, Phys. Rev. Lett. **85**, 4932 (2000).

[34] L. Berger, Phys. Rev. B **2**, 4559 (1970).

[35] J. M. Luttinger, Phys. Rev. **112**, 739 (1958).

[36] J. Smit, Physica **21**, 877 (1955).

[37] J. Smit, Physica **24**, 39 (1954).

[38] A. Fert and O. Jaoul, Phys. Rev. Lett. **28**, 303 (1972); T. Okamoto, H. Tange, A. Nishimura, and E. Tatsmoto, J. Phys. Soc. Jpn. **17**, 717 (1962); G. C. Carter and E. M. Pugh, Phys. Rev. **152**, 498 (1966); M. Ziese and C. Srinitiwarawong, Europhys. Lett. **45**, 256 (1999).

[39] P. Wagner, I. Gordon, A. Vantomme, D. Dierickx, M. J. Van Beal, V. V. Moshchalkov, and Y. Bruynseraede, Europhys . Lett. **41**, 49 (1998).

[40] T. Jungwirth, Q. Niu, and A. H. MacDonald, Phys. Rev. Lett. **88**, 207208 (2002).

[41] Y. Yao, L. Kleinman, A. H. MacDonald, J. Sinova, T. Jungwirth, D.-S. Wang, E. Wang, and Q. Niu, Phys. Rev. Lett. **92**, 037204 (2004).

[42] M. V. Berry, Proc. R. Soc. Lond. A **392**, 45 (1984).

[43] Z. Fang, N. Nagaosa, K. S. Takahashi, A. Asamitsu, R. Mathieu, T. Ogasawara, H. Yamada, M. Kawasaki, Y. Tokura, and K. Terakura, Science **302**, 92 (2003).

[44] Y. Kats, I. Genish, L. Klein, J. W. Reiner, and M . R. Beasley, Phys. Rev. B **70**, 180407(R) (2004).

[45] L. Klein, J. W. Reiner, T. H. Geballe, M. R. Beasley, and A. Kapitulnik, Phys. Rev. B **61**, R7842 (2000).

[46] A. Gerber, A. Milner, L. Goldshmit, M. Karpovski, B. Lemke, H.-U. Habermeier, and A. Sulpice, Phys. Rev. B **65**, 054426 (2002).

[47] J.M. Ziman, Principles of the Theory of solids, Cambridge University Press, Cambridge, 1972, pp. 250-254.

[48] J. Smit, Physica (Amsterdam) **17**, 612 (1951).

[49] C. B. Eom, R. J. Cava, R. M. Fleming, J. M. Fillips, R. B. vanDover, J. H. Marshal, J. W. P. Hsu, J. J. Krajewski, and W. F. Peck, Sience **258** 1766 (1992).

[50] Q. Gan, R. A. Rao, C. B. Eom, L. Wu, and F. Tsui, J. Appl. Phys. **85**, 5297 (1999).

[51] L. Klein, J. S. Dodge, C. H. Ahn, G. J. Snyder, T. H. Geballe, M. R. Beasley, and A. Kapitulnik, Phys. Rev. Lett. **77**, 2774 (1996).

[52] L. Klein, J. S. Dodge, C. H. Ahn, J. W. Reiner, L. Mieville, T. H. Geballe, M. R. Beasley, and A. Kapitulnik, J. Phys.: Condens. Matter **8**, 10111 (1996).

[53] L. Klein Y. Kats, N. Wiser, M. Koncczykowski, J. W. Reiner, T. H. Geballe, M. R. Beasley, and A. Kapitulnik, Europhys. Lett. **55**, 532 (2001).

[54] Y. Kats, and L. Klein, Phisica B **312-313**, 793 (2002).

[55] A. P. Mackenzie, J. W. Reiner, A. W. Tyler, L. M. Galvin, S. R. Julian, M. R. Beasley, T. H. Geballe, and A. Kapitulnik, Phys. Rev. B **58**, R13318 (1998).

[56] G. Cao, S. McCall, M. Shepard, J. E. Crow, and R. P. Guertin, Phys. Rev. B **56**, 321 (1997).

[57] M. Shepard, S. McCall, G. Cao, and J. E. Crow, J. Appl. Phys. **81**, 4978 (1997).

[58] T. C. Gibb, R. Greatrex, N. N. Greenwood, and P. Kaspi, J. Chem. Soc. (Dalton Trans.) **12** 1253 (1973).

[59] M. Shepard, G. Cao, S. McCall, F. Freibert, and J. E. Crow, J. Appl. Phys. **79**, 4821 (1996).

[60] G. Cao, F. Freibert, and J. E. Crow, J. Appl. Phys. **81**, 3884 (1997).

[61] J. M. Longo, P. M. Raccah, and J. B. Goodenough, J. Appl. Phys. **39**, 1327 (1968).

[62] A. Kanbayasi, J. Phys. Soc. Jpn. **44**, 108 (1978).

[63] I. Felner, I. Nowik, I. Baradic, and M. Gospodinov, Phys. Rev. B **62**, 11332 (2000).

[64] F. Ricci, M. F. Bevilacqua, F. Miletto Granozio, and U. Scotti di Uccio, Phys. Rev. B **65**, 155428 (2002).

[65] Y. S. Lee, J. Yu, J. S. Lee, T. W. Noh, T. H. Gimm, H.Y. Choi, and C. B. Eom, Phys. Rev. B **66**, 41104 (2002).

[66] G. Cao, O. Korneta, S. Chikara, L. E. DeLong, and P. Schlottmann; e-print: cond-mat/0805.0741.

[67] G. Cao, V. Duarairaj, S. Chikara, L. E. Delong, S. Parkin, and P. Schlottmann, Phys. Rev. B **76**, 100402(R) (2007).

[68] T. Kiyama, K. Yoshimura, and K. Kosuge, H. Michor, and G. Hilscher, J. Phys. Soc. Jpn. **67**, 307 (1998).

[69] T. Kiyama, K. Yoshimura, and K. Kosuge, J. Phys. Soc. Jpn. **68**, 3372 (1999).

[70] T. He, and R. J. Cava, Phys. Rev. B **63**, 172403 (2001).

[71] P. Khalifah, I. Ohkubo, H. M. Christen, and D. G. Mandrus, Phys. Rev. B. **70**, 134426 (2004).

[72] N. Shanthi and D. D. Sarma, Phys. Rev. B **57**, 2153 (1998).

[73] L. F. Mattheiss, Phys. Rev. B **6**, 4718 (1972).

[74] M. A. Saifi and L. E. Cross, Phys. Rev. B **2**, 677 (1970).

[75] J. H. Barrett, Phys. Rev. **86**, 118 (1952).

[76] D. Fuchs, C. W. Schneider, R. Schneider, and H. Rietschel, J. Appl. Phys. **85**, 7362 (1999).

[77] A. Ohtomo and H. Y. Hwang, Nature **427**, 423 (2004).

[78] H. Y. Hwang, A. Ohtomo, N. Nakagawa, D. A. Muller, and J. L. Grazul, Physica E **22**, 712 (2004).

[79] S. Thiel, G. Hammerl, A. Schmehl, C. W. Schneider, and J. Mannhart, Science, **313**, 1942 (2006).

[80] A. S. Kalabukhov, R. Gunnarsson, J. Börjesson, E. Olsson, T. Claeson, and D. Wingler, Phys. Rev. B **75**, 121404(R) (2007).

[81] W. Siemons, G. Koster, H. Yamamoto, T. H. Geballe, D. H. A. Blank, and M. R. Beasley, Phys. Rev. B **76**, 155111 (2007)

[82] G. Herranz, M. Basletic, M. Bibes, C. Carretero, E. Tafra, E. Jacquet, K. Bouzehouane, C. Deranlot, J.-L. Maurice, A. Hamzic, J. P. Contour, A. Barthélémy, and A. Fert, cond-mat/0704.2523.

[83] D. M. Newns, J. A. Misewich, C. C. Tsuei, A. Gupta, B. A. Scott, and A. Schrott, Appl. Phys. Lett. **73**, 780 (1998).

[84] I. Pallecchi, G. Grassano, D. Marré, L. Pellegrino, M. Putti, and A. S. Siri, Appl. Phys. Lett. **78**, 2244 (2001).

[85] K. Ueno, I. H. Inoue, H. Akoh, M. Kawasaki, Y. Tokura, and H. Takagi, Appl. Phys. Lett. **83**, 1755 (2003).

[86] O. N. Tufte and P. W. Chapman, Phys. Rev. **155**, 796 (1967).

[87] K. Szot, W. Speier, R. Carius, U. Zastrow, and W. Beyer, Phys. Rev. Lett. **88**, 075508 (2002).

[88] H. P. R. Frederikse, W. R. Thurber, and W. R. Hosler, Phys. Rev. **134**, A442 (1964).

[89] V. E. Henrich, G. Dresselhaus, and H. J. Zeiger, Phys. Rev. B 17, 4908 (1978).

[90] D. W. Reagor and V. Y. Butko, Nature Materials **4**, 593 (2005).

[91] D. Kan, T. Terashima, R. Kanda, A. Masuno, K. Tanaka, S. Chu, H. Kan, A. Ishizumi, Y. Kanemitsu, Y. Shimakawa, and M. Takano, Nature Materials **4**, 816 (2005).

[92] J. W. Reiner, Ph.D. Thesis, Stanford University, 2002.

[93] J. M. E. Harper, J. J. Cuomo, and H. R. Kaufman, J. Vac. Sci. Technol, **21**, 737-756 (1982).

[94] M. B*ü*ttiker, Phys. Rev. Lett. **57**,1761 (1986).

[95] M. B*ü*ttiker, IBM J. Res. and Dev. **50**, 101 (2006).